minerals

MDPI

Article

Strategies for Targeting in Undercover Terrains: Modeling Multi-Source Data in Apuí Region, SW Amazon Craton, Brazil

Lila Costa Queiroz [1,2,*], Adalene Moreira Silva [1], Frederico Ricardo Ferreira Rodrigues de Oliveira e Sousa [2,*], Michele Zorzetti Pitarello [2] and Márcia Abrahão Moura [1]

[1] Instituto de Geociências, Campus Universitário Darcy Ribeiro, Universidade de Brasília, Brasília 70910-900, Brazil
[2] GSB/CPRM—Geological Survey of Brazil, Brasília 70040-904, Brazil
* Correspondence: lila.queiroz@sgb.gov.br (L.C.Q.); frederico.oliveira@sgb.gov.br (F.R.F.R.d.O.e.S.)

Abstract: Exploring covered terrains is a challenge that requires the integration of multiple sources of knowledge, particularly in the initial stages of mineral exploration. The Apuí region, located in the Southwestern Amazon Craton, has a small and constant gold production, despite the deep cover and limited geological knowledge. The gold is mainly hosted in quartz veins and breccias that cut Paleoproterozoic volcano-sedimentary sequences. The occurrences have similar characteristics to magmatic–hydrothermal deposits, such as a lack of regional metamorphism and intense hydrothermalization. We undertook a multi-source prospective investigation on different scales using 2D and 3D techniques to translate the footprints of the mineral system into mappable criteria. Gold prospectivity maps for the Juma District and Guida Target were produced by integrating geological, geochemical, and geophysical datasets in knowledge-driven fuzzy systems. Regional airborne magnetization vector inversion (MVI) models were utilized. The correlation between the drill cores and the magnetic susceptibility models highlighted a potential surface for gold mineralization associated with the boundary between a granitic intrusion and volcano-sedimentary rocks. The prospectivity maps reduced the search area, and the regional susceptibility models allowed for the reconnaissance of structures and bodies that may be related to gold mineralization at depth. The results present new strategies for increasing discovery performance in the Southern Amazon Craton under cover.

Keywords: mineral prospectivity mapping (MPM); Amazon Craton; fuzzy logic; airborne geophysics; magnetization vector inversion (MVI)

check for updates

Citation: Queiroz, L.C.; Silva, A.M.; e Sousa, F.R.F.R.d.O.; Pitarello, M.Z.; Moura, M.A. Strategies for Targeting in Undercover Terrains: Modeling Multi-Source Data in Apuí Region, SW Amazon Craton, Brazil. *Minerals* **2023**, *13*, 78. https://doi.org/10.3390/min13010078

Academic Editor: Behnam Sadeghi

Received: 4 November 2022
Revised: 28 December 2022
Accepted: 30 December 2022
Published: 4 January 2023

Copyright: © 2023 by the authors. Licensee MDPI, Basel, Switzerland. This article is an open access article distributed under the terms and conditions of the Creative Commons Attribution (CC BY) license (https://creativecommons.org/licenses/by/4.0/).

1. Introduction

Targeting mineral deposits in undercover terrains requires the integration of multiple techniques over various scales for effective results. In recent decades, studies on the lithosphere, which is associated with the mineral system concept, has provided valuable information as regards potential hidden deposits [1–3]. Carranza [4] and Kreuzer et al. [5] expanded the discussion on how to manage and use multiple sources of data to obtain meaningful geological information in mineral prospectivity mapping (MPM). Shirazi et al. [6] applied geostatistical and remote sensing studies to define potential metallogenetic regions. More recently, Yousefi et al. [7] presented an overview of the data analysis methods for MPM, identifying significant deficiencies and discussing possible solutions for improving 2D targeting science. González-Álvarez et al. [8] discussed a wide variety of research focused on regions in which mineral deposits are under cover, reflecting a global trend of progressively exploring deeper. Using multiple geophysical methods along with geology and geochemistry has become fundamental in finding new deposits in regions with deep weathered cover, particularly in tropical environments. Joly et al. [9] suggested that knowledge-driven methods [10] should be carried out prior to data-driven methods in the first stages of mineral exploration to avoid undesirable bias. As mentioned by Porwal

et al. [11], in prospectivity modeling, the judgment is commonly overly influenced by the geological characteristics of the known deposits and the location of targets generated by previous data-driven approaches.

In the Amazon Craton, the expansion of the geophysical coverage allowed for the mapping of important structures and our understanding of the regional framework. Seismological and gravimetric models suggest that the crustal thickness in the Amazon Craton is quite variable [12–14]. Albuquerque et al. [14] defined the range of crustal thickness to be approximately 29–56 km, with an average thickness of 38.2 km. Albuquerque et al. [14] and Lloyd et al. [15] showed that it was not possible to correlate the geochronology of the Amazon Craton provinces and their crustal thicknesses. There are regions of thicker crust in younger provinces, such as the Rondônia-Juruena region, and thinner crust in older provinces, such as the Central Amazon. The integration of the Geological Survey of Brazil (GSB) potential field database, including airborne geophysics and gravimetric surveys, showed that the limits between the geochronological provinces in Southern Amazon Craton are still unclear and possibly gradational.

The Apuí region, our case study in this work, is located in the Southern Amazonas state, Brazil. Since the 1970s, the area has had constant gold production via artisanal mining. In 2006, the discovery of the Garimpo Eldorado do Juma increased the prospective interest in the region despite limited geological and geotectonic knowledge. The occurrence of Orosirian granites in the Juma District indicates a geological context in which rocks from Rondônia-Juruena Province are in contact with rocks from Tapajós-Parima Province, similar to the Peixoto de Azevedo Domain [16,17]. Meloni et al. [18] characterized the metallogenesis and geotectonic evolution of the Juma District (also known as Eldorado do Juma District or Juma Gold District), including prospective implications for epithermal gold prospection. The majority of the gold occurrences exhibit characteristics of magmatic–hydrothermal systems that, in some cases, are similar to regionally correlated deposits, notably from the Alta Floresta and Tapajós Mineral Provinces (e.g., [19–21]).

This work presents an overview of the geological setting and mineralization of the Apuí region, revealing key geological, geophysical, geochemical, and structural factors for discovering hidden gold deposits. On the basis of a magmatic–hydrothermal exploratory model, we used new strategies to solve the problem of mineral exploration in regions with thick and intensely weathered cover. This was undertaken on different scales to translate the footprints of the mineral system into mappable criteria by applying 2D and 3D techniques. Prospectivity maps, based on fuzzy logic, highlighted favorable areas for undiscovered gold deposits in the Juma District. A regional magnetization vector inversion (MVI) model constrained targets to an estimated depth of 20 km, supporting the reconnaissance of bodies and structures that possibly control the fluid pathways and deposition. The analysis of six drill cores combined with the magnetic susceptibility models allowed for the delineation of a surface interpreted as the contact between a granite intrusion and the volcano-sedimentary basement. We define this zone as a high potential location for host gold occurrences.

2. Geological Setting and Mineralization

The Amazon Craton is the largest pre-Cambrian exposure in the South American Platform [22]. Defined as the portion of the continental crust that remained stable during the Brasiliano Orogeny [23,24], the craton evolution is marked by successive accretionary events, from Paleo- to Neoproterozoic [25–27]. On the basis of U-Pb and Sm-Nd isotope geochemistry, the units progressively get younger from east to west [28,29]. The Paleoproterozoic units in the Amazon Craton are recognized for hosting significant gold deposits, the largest and most studied are located in the Tapajós and Alta Floresta Mineral Provinces. The total gradient (TG) of total magnetic intensity (TMI) illustrates a regional continuity in the structural framework and similar geophysical responses in adjacent geochronological provinces, suggesting a gradational transition between them (Figure 1a). Geochronological data, compiled from the GSB and [27], combined with the Bouguer anomaly map

(WGM2012) [30] show that the relationship between ages, geological domains, and crust density remains unclear for the Southern Amazon Craton (Figure 1b).

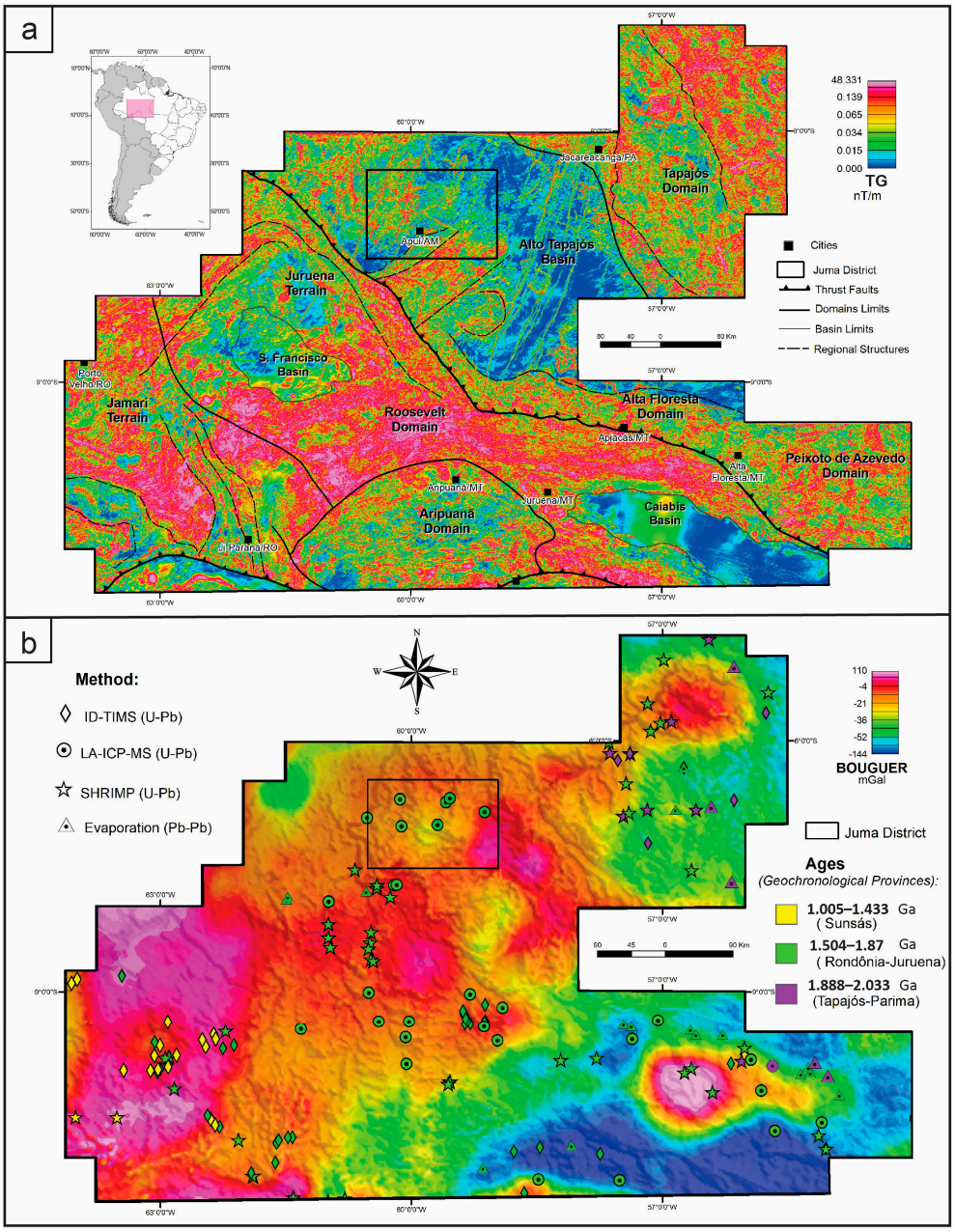


Figure 1. Airborne magnetic and satellite gravimetric maps for the Southern Amazon Craton; (**a**) Major structures and domains superimposed on the total gradient (TG) of total magnetic intensity (TMI); (**b**) geochronological data compiled from the Geological Survey of Brazil (GSB) and [27] on the Bouguer anomaly map (WGM2012) [30].

2.1. Juma District Geology

The Juma District is located in the SW Amazon Craton, covering an area of 18,000 km^2 that records Paleoproterozoic to Paleozoic geologic events (Figure 2). The volcano-sedimentary sequences from the Rondônia-Juruena Province (1.82–1.53 Ga; [29,31]) cover most of the area. The basement is interpreted as Orosirian metasedimentary rocks from the Abacaxis Formation [29] cut by the Chuim (1.85 Ga) and Arraia (1.83 Ga) porphyritic granites [17,18]. The Colíder Group [32] dominantly overlaps the basement with silicic volcanic rocks (1.81–1.76 Ga; [17,33,34]). The majority of the Juma District area is covered by the volcano-

sedimentary Beneficente Group (*sensu* [35]), interpreted as a rift-type basin (~1.74–1.6 Ga) with volcanism that juxtaposes the Colíder Group [17]. After deposition, low-grade metamorphism and structural relief features affected the sequences between 1.5 and 1.4 Ga [36]. On the basis of detailed stratigraphic studies, Simões et al. [17] divided the Beneficente Group into three formations: Pedro Sara, Camaiú, and Vila do Carmo. At the base of the succession, the Pedro Sara Formation is composed of silicic volcanic rocks covered by conglomerates and sandstones interleaved with basaltic rocks from the Camaiú Formation. The Vila do Carmo member is an intercalation of pelites, sandstones, and rare tuffs, representing the final stage of the Beneficente sedimentation. Mesoproterozoic gabbro sills from the Matá-Matá Suite [37] cut all the volcano-sedimentary sequences mentioned. The Paleozoic sedimentary rocks from the Alto Tapajós Basin are exposed in the topographically lower regions.

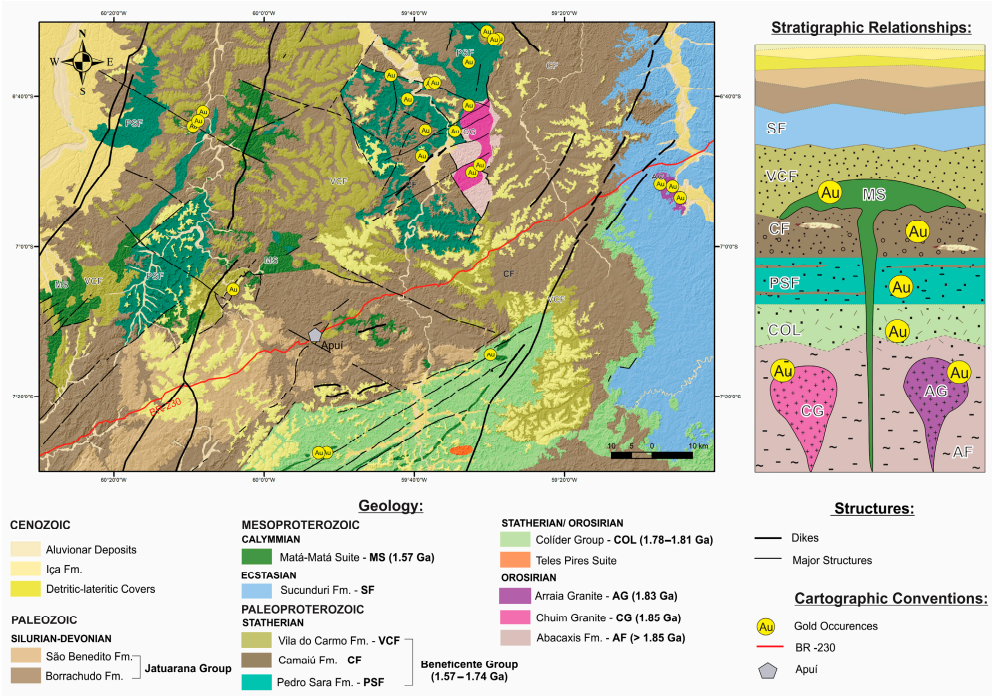


Figure 2. Juma District geological map with the location of gold occurrences, major regional structures, and the main road (BR-230). The stratigraphic relationships section illustrates that gold occurrences are associated with Orosirian to Mesoproterozoic rocks (modified from Meloni et al. [18]). Abbreviation: Fm.—formation.

2.2. Gold Mineralization

This study considered 24 gold occurrences in the Juma District (Figure 2), the majority corresponding to artisanal prospects, including 16 primary deposits. Considering the spatial distribution and geologic characteristics, we defined two types of gold occurrences for the Apuí region. The first type is associated with the Orosirian Chuim and Arraia granites, possibly related to a magmatic-arc environment with a dominantly compressive ductile tectonic regime. The second type is characterized by a strong structural control associated with at least two mineralized events from Paleo- to Mesoproterozoic.

In the first type, gold occurs in quartz veins or hydrothermal breccias with siliceous matrices, occasionally exhibiting drusiform, microcrystalline, and lattice-bladed textures [18,38]. Meloni et al. [18] described typical features of low-sulfidation epithermal systems, such as breccias containing placoid calcite pseudomorphs replaced by quartz. Sulfide is uncommon but can be locally associated with mineralization. Hydrothermal alteration halos are evidenced by chloritization, carbonation, sericitization, quartz-adularia veins, and clay minerals. The Chuim and Arraia granites have similarities in age and chemistry with the granites from the Matupá Suite, particularly the Serrinha gold deposit in the Alta Floresta

Mineral Province [19,39,40] (Table 1). Certain geologic characteristics are also similar to the Tocantinzinho Deposit in Tapajós Domain [41,42], and to porphyry gold deposits compiled from [43–47], as detailed in Table 1. The apparent absence of regional metamorphism in the host rocks and the correspondence with the literature are consistent with a magmatic–hydrothermal origin for the gold, with similarities to porphyry–epithermal systems.

Table 1. Key characteristics of the Juma District Orosirian gold deposits compared to the Serrinha, Tocantinzinho, and porphyry gold deposits (Adapted from [19,42]).

	Juma District	Serrinha Deposit	Tocantinzinho Deposit	Porphyry Gold Deposits
Tectonic Environment	Magmatic arc	Volcano-plutonic arc	Magmatic arc	Volcano-plutonic arc
Intrusion Age	1855.1 ± 6.4 Ma (Chuim Granite); 1837.8 ± 9.6 Ma (Arraia Granite)	1872 ± 12 Ma	1982 ± 8 Ma	Variable, predominantly Cenozoic and Mesozoic
Host rock composition	I- and S-type, peraluminous and magnesian, calc-alkaline to alkali-calcic, porphyritic monzogranite	I-type, magnetite-series, equigranular to porphyritic monzogranite cut by cogenetic rhyolitic dikes	I-type, calc-alkaline, magnetite-series, oxidized, monzogranite	I-type, magnetite-series porphyry; coeval volcanic rocks are common
Mineralization type	Quartz veins, breccias, and stockworks	Disseminated	Disseminated; in veinlets and fractures (stockwork)	Disseminated; stockwork; fractures controlled
Main metals	Au	Au	Au	Au-(Cu)
Key sulfides associated	±Pyrite	Pyrite	Pyrite	Pyrite-(chalcopyrite; bornite)
Association of hydrothermal alteration	Epidote, actinolite, chlorite, calcite, sericite, adularia, florencite	K-feldspar, albite, chlorite, sericite, pyrite, magnetite	Phyllic alteration, K-feldspar alteration (microclinization)	Biotite, K-feldspar, magnetite, sericite, anhydrite, albite, pyrite, chlorite, clay
References	[16,18,38]	[19,39,40]	[41,42]	[43–47]

The second type is associated with regional ductile to brittle fault corridors and shear zones, preferentially NE–SW, E–W, and NW–SE. These structures could be associated with the emplacement of igneous intrusions. The most important structural domain is a NE–SW deep shear zone that cuts the southeastern Juma District and allocates gold occurrences (notably, the Ema and Três Estados prospects from BBX Minerals). The gold is typically hosted in lapilli-tuffs and diabases associated with quartz veins. In the Garimpo Eldorado do Juma cluster of occurrences, the gold is widespread in networks and stockworks of hydrothermal kaolinite veinlets, millimeters to a centimeter in size, which cut the volcano-sedimentary strata [18,48,49]. In this case, silicification is subordinate, quartz veins are uncommon, and argilization, probably from a hydrothermal origin superimposed by weathering, totally alters the feldspars in phenolatites [18]. Frequently, millimeter rosettes of tourmaline occur within the altered feldspar crystals [49]. The occurrences are interpreted as epigenetic and occur preferentially in the geological contact between the Matá-Matá gabbros and the Beneficent/Colíder Groups. At least two mineralization events produced these types of gold occurrences. The first is related to rifting with bimodal volcanism and hydrothermal activity at ~1.70 Ga [17,18]. The other is related to the gold occurrences in association with mafic rocks from the Matá-Matá Suite, indicating that at least one mineralization event affected the area in the Mesoproterozoic.

3. Materials and Methods

In this research, an integrated methodology is proposed for mapping the expressions of a magmatic–hydrothermal gold mineral system at different scales. The work was divided into four stages: (1) input data selection; (2) data processing; (3) 2D targeting using mineral prospectivity maps (MPM); (4) 3D airborne magnetic data inversion and correlation with known geology. Figure 3 illustrates all the stages, including the main processes and data employed in this study.

The methodology was expanded and modified from previous works [2,50–55]. Hronsky and Groves [2] followed by Hagemann et al. [50] defined the scale dependency of exploration targeting criteria as a critical aspect of effectiveness when applying the mineral system concept to prospectivity modeling. The techniques and main steps we used to translate the footprints of the mineral systems into mappable criteria were adapted from Pan and Harris [51] and Harris et al. [52], and further adapted by Nykänen [53]. Silva et al. [54] modified the previous methods for undercover gold targeting in the Southern Amazon Craton, including a drilling program for target testing. Uchôa et al. [55] expanded the prospective studies with multi-process and multi-scale spatial predictive analyses for orogenic gold.

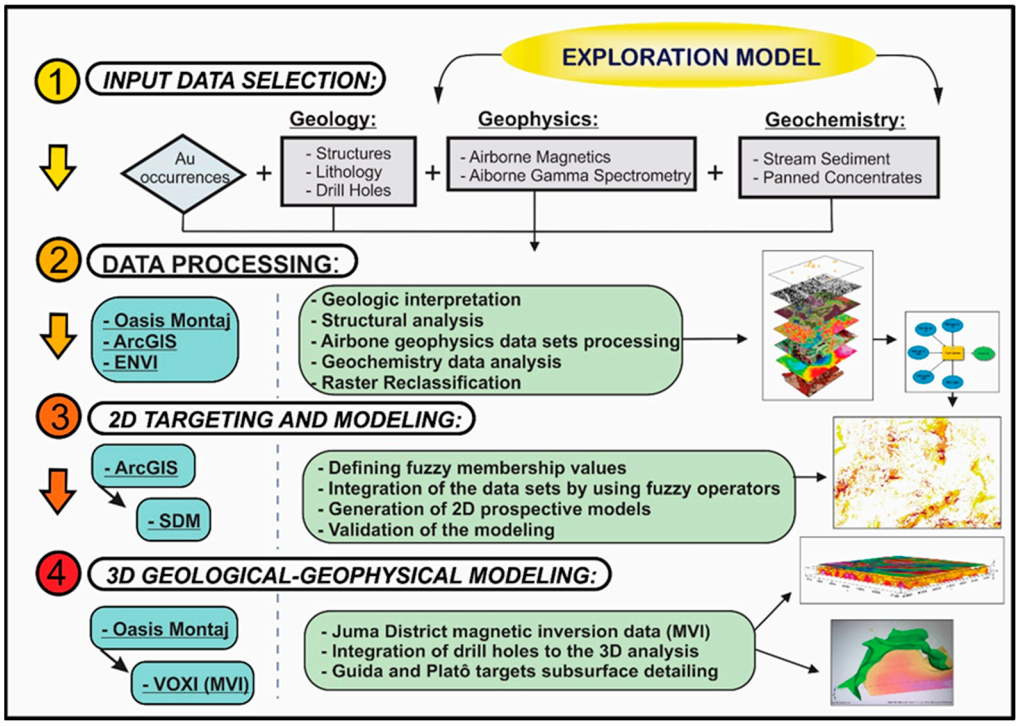


Figure 3. Flowchart illustrating the main steps and products generated for this work, based on the methodologies of Pan and Harris [51], Harris et al. [52], and modified after Nykänen [53] and Silva et al. [54].

3.1. Datasets

The dataset consists of multi-source georeferenced layers, including known gold occurrences, the Juma District geological map, airborne magnetic and radiometric surveys, the mineralogy of panned concentrates, and a geochemical analysis of stream sediment samples. The Geological Survey of Brazil (GSB) provided the geographical information system (GIS) database. In addition, six drill cores acquired by the company BBX Minerals, varying in depth from 180 to 300 m, were utilized in this study. Airborne magnetic, radiometric, and satellite gravimetric data were also considered. The airborne magnetic and radiometric surveys were acquired in N–S lines flown at 500 m spacings with a constant 100 m flight height.

The geochemical and mineralometric surveys comprise the analysis of 485 samples of active stream sediments (<80#) and 484 samples of heavy mineral concentrate, covering 2/3 of the Juma District area. The distribution of samples approximately corresponds to a 1:100,000 scale, with a maximum density of one sample every 10 km^2. All samples, from both matrices, were prepared and analyzed by SGS-Geosol laboratories. The complete data analysis is available in [18,56].

The preparation of stream sediment samples involved (i) oven drying at 60 degrees; (ii) sieving in <80# fraction; (iii) pulverization and; (iv) digestion by aqua regia (HNO_3 + 3HCl). The analyses were performed on ICP-OES (inductively coupled plasma optical emission, PerkinElmer Inc., Waltham, MA, USA) and ICP-MS (inductively coupled plasma mass spectrometry, PerkinElmer Inc., Waltham, MA, USA) for 51 elements: Ag, Al, As, Au, B, Ba, Be, Bi, Ca, Cd, Ce, Co, Cr, Cs, Cu, Fe, Ga, Ge, Hf, Hg, In, K, La, Li, Mg, Mn, Mo, Na, Nb, Ni, P, Pb, Rb, Re, S, Sb, Sc, Se, Sn, Sr, Ta, Te, Th, Ti, Tl, U, V, W, Y, Zn, and Zr. Quality control was performed by inserting a blank reference material and replicates. Duplicates of stream sediment samples were collected every ten samples.

Heavy mineral samples were collected by panning 20 L of sand/gravel in the same location as the stream sediment samples. The preparation consisted of sieving, quartering, and separation by density and by magnetism. The remaining minerals were analyzed using a binocular loupe and an optical microscope. Semi-quantitative results of heavy mineral concentrates are expressed as a percentage in the following ranges <1%, 1%–5%, 5%–25%, 25%–50%, 50%–75%, and 75%–100%, and comprised more than 30 minerals including silicates, sulfates, phosphates, oxides, and others. Gold was the only mineral quantitatively analyzed after quartering.

3.2. Data Processing

For the airborne magnetic data, the International Geomagnetic Reference Field (IGRF) correction was performed. Then, the data were interpolated using the bi-directional method to obtain the total gradient (TG) of the total magnetic intensity (TMI) and its products. The radiometric data were pre-processed to eliminate inconsistent and negative values. The K, eTh, and eU channels were interpolated using the minimum curvature method [57,58]. The eU and eTh maps were expressed as equivalent values (ppm) and K as percentages. The main products developed are the radioelement ratios, ternary false-color RGB composition, F factor (F = K × (eU/eTh) [59]), and anomalous K [60].

The geochemistry data were log-transformed to approximate a normal distribution. Previously, data below the lower detection limit (LDL) were transformed to values corresponding to LDL × 0.5. Au, B, Ge, and Re showed no value above the LDL and were not used. The database was then processed by univariate statistical techniques for geochemical data [61–65]. The values were classified between anomalies and background for each element, defined according to the classes of their respective box-whiskers plots. Anomalous values were considered as: (i) third order, above Q3 + (1.5 × Q3 − Q1); (ii) second order, above Q3 + (3 × Q3 − Q1); and (iii) first order, above Q3 + (4.5 × Q3 − Q1), where Q3 represents the 75% quartile (3rd) and Q1 the 25% quartile (1st). Third-order positive anomalies occurred for 24 elements: Al, Ba, Ca, Cd, Ce, Co, Cs, Cu, Fe, Ga, Hf, K, La, Li, Mg, Mn, Nb, Ni, Rb, Sc, Sr, Th, U, and Y. Second-order positive anomalies occurred for 7 elements: Cr, In, Mo, Pb, Sb, Sn, and W; and first-order anomalies occurred for 3 elements: Sb, Sn, and W. The spatial distributions are shown through uni-elementary maps of the corresponding hydrographic basins for each sample. The statistical summary for various elements considered relevant in this analysis is available in Table S2 (Supplementary Materials).

The mineralometric data (heavy minerals) were also plotted as hydrographic basin maps, classified according to the percentage ranges provided by the laboratory analyses, with the exception of gold, which was classified according to the absolute number of grains. The spatial distribution is shown through uni-elementary maps of the corresponding hydrographic basins for each sample (Figure 4).

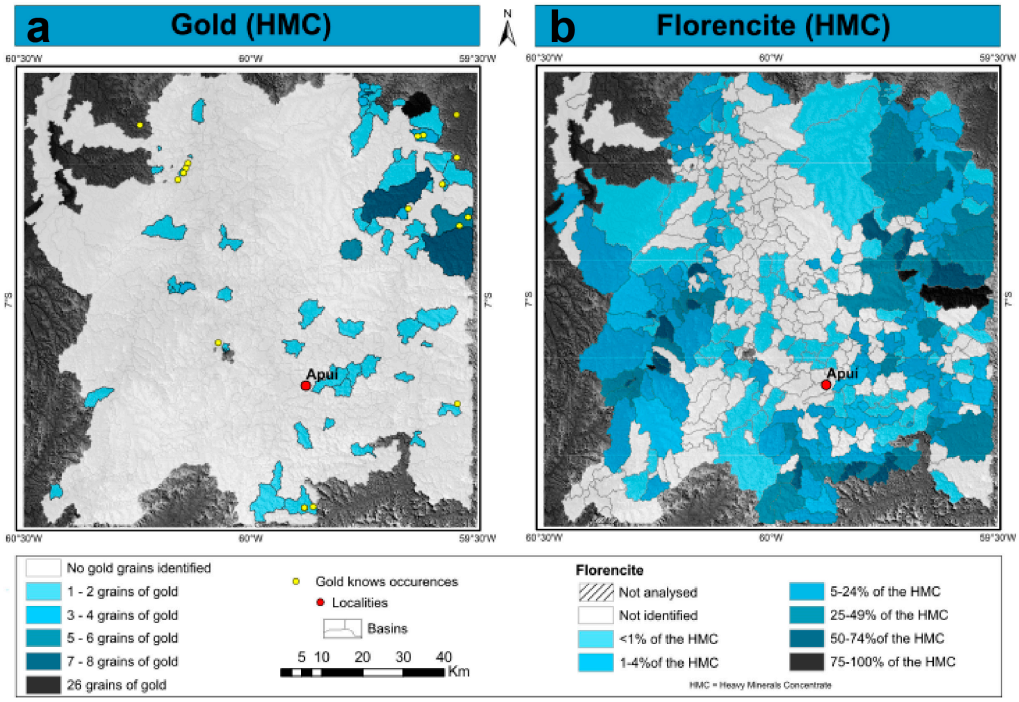


Figure 4. Spatial distributions for heavy mineral concentrates (HMC) are shown through maps of the corresponding hydrographic basins for each sample; (**a**) Gold HMC; (**b**) Florencite HMC.

3.3. Mineral Prospectivity Mapping (MPM)

MPM applies a probabilistic targeting approach to refining the exploration model into spatial proxies. To map the footprints of the mineral system, we defined three main elements: the source, migration, and depositional processes, adapted from [50]. Understanding how these elements act was an effort undertaken on different scales, which indicated the main exploration vectors for the Apuí region. The spatial proxies were obtained from the geology, structures, airborne geophysics, and surveys from stream sediment and heavy mineral concentrates. Our approach was applied at two scales: 1:250,000 for the Juma District and 1:100,000 for the Guida Target.

We applied fuzzy systems to produce the Juma District and Guida Target prospectivity maps. Fuzzy logic is a many-valued logic based on the mathematical fuzzy-set theory, initially proposed by [66]. In mineral exploration, this logic has been applied to prospectivity maps, usually in knowledge-driven models. Several geoprocessing techniques were required, including interpolation, raster calculation, image processing, and classification. Then, the fuzzification stage consisted of choosing the most appropriate fuzzy memberships for each layer, i.e., a standardized simplification of different data to allow them to be used together. The pertinence functions used in this work were the fuzzy categorical (in which the expert defines the values to be highlighted), fuzzy small (which highlights the smallest values), and fuzzy large (which highlights the largest values). After this stage, the critical mineralization parameters were transformed into evidential maps using the most appropriate fuzzy operators, resulting in values that vary from 0 (strongly negative evidence) to 1 (strongly positive evidence). We used the operators fuzzy AND, fuzzy OR, and fuzzy Gamma. The fuzzy AND operator is an intersection function whose results tend toward conservative values, while fuzzy OR is a maximum operator that tends toward larger values. The fuzzy Gamma operator combines the fuzzy sum and fuzzy product [67]. Figures 5 and 6 illustrate the steps for Juma District and Guida Target prospectivity modeling.

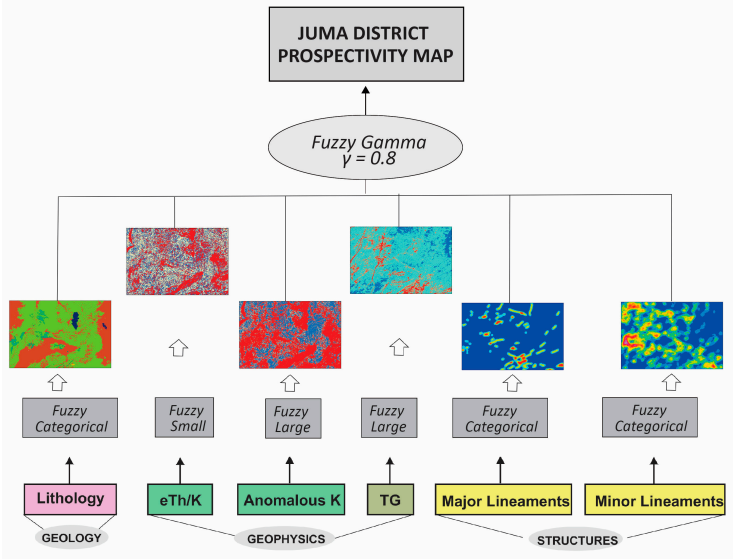


Figure 5. Flowchart detailing the main steps for Juma District prospectivity modeling, including the fuzzy logic operators and pertinence functions.

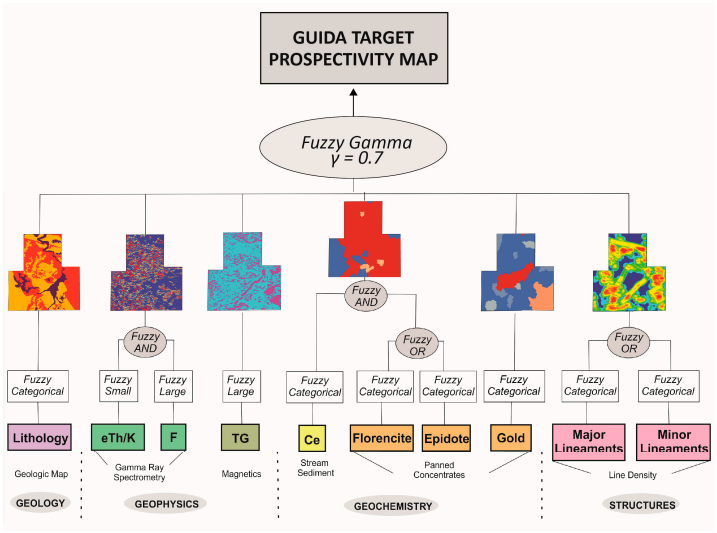


Figure 6. Flowchart detailing the main steps for Guida Target prospectivity modeling, including the fuzzy logic operators and pertinence functions.

3.4. Magnetization Vector Inversion (MVI)

Magnetization vector inversion (MVI) is a computational algorithm designed to generate 3D models for magnetic susceptibility and magnetization vectors, considering the effects of induced and residual magnetization. Ellis et al. [68] mathematically describe the MVI method, based on Tikhonov regularization, to solve the inverse problem for the magnetization vector by minimizing the difference between the calculated and the measured field. Conventional 3D magnetic susceptibility inversions assume that there is no remanent magnetization and that the induced magnetization is always in the same direction as the Earth's magnetic field. However, in practice, this assumption is not always valid. The MVI enables the magnetization direction and amplitude to be recovered for each magnetic domain in the survey area [68]. In mineral exploration, recent studies have applied MVI to obtain the subsurface three-dimensional distribution, the position, the magnetization magnitude, and the direction of magnetic targets with remanence (e.g., [69]).

4. Results

4.1. Juma District Spatial Proxies

The critical processes identified for the gold system in the Juma District were translated into spatial proxies for use in knowledge-driven prospectivity models. Six evidential maps, compatible with the 1:250,000 scale, were extracted from geological, structural, and airborne magnetic and radiometric data. The gold system was translated into three system components: source (region/fertility), fluid pathways (conduits), and deposition (evidence of hydrothermal alteration processes).

To map the source of the gold, the geological units were classified considering their affinity to the gold. The units that showed a temporal-spatial relationship to known gold occurrences received the highest weights, such as the Orosirian granites and mafic rocks from the Matá-Matá Suite. In contrast, the Paleozoic units received smaller weights since the mineralization events were older. The proximity to geologic structures was the main spatial proxy for mapping the fluid conduits since they tend to flow by faults, shears, thrusts, lithological contacts, and fold axes. As mineralization is expected to occur in spatial proximity to or at the intersection of structures, we applied the kernel density algorithm to generate two evidential maps for minor and major structures, in which the denser regions are considered the most prospective. We opted to use the total gradient (TG) considering the highest values as spatial proxies since the geological structures associated with the mineralization frequently exhibited positive magnetic signatures on the province scale. We also used airborne magnetic products to support mapping lineaments and features that may act as pathways for the gold. Hydrothermal alteration plays an important role in gold deposition since it tends to concentrate and precipitate fluids. In the Juma District, the K-enriched areas act as an indicator of this remobilization. The eTh/K and anomalous K maps were processed to highlight the largest values, which are considered a proxy for gold remobilization and deposition. In Table 2, the theoretical fundamentals, spatial proxies, primary data, and evidential maps are described for each exploratory criterion (geological, structural, and geophysical).

Table 2. Key characteristics describing the theoretical fundamentals, spatial proxies, primary data, and evidential maps using different exploratory criteria for the Juma District.

Exploratory Criteria	Fundamentals	Spatial Proxies	Primary Data	Evidential Maps
Geological	Gold is mainly hosted by non-metamorphic Paleo-Mesoproterozoic rocks from volcano-sedimentary sequences or associated with Orosirian granites; hydrothermal alteration is common	Paleo- Mesoproterozoic igneous and volcano-sedimentary rocks; hydrothermal alteration zones	Juma District geological map; geochronological data	(1) Lithological units weighted by the prospective potential to host gold
Structural	Lineaments and faults could act as structural controls for fluids	Proximity to faults and lineament; structures intersection	Airborne magnetic data; Juma District geological map	(2) Major lineaments density (3) Minor lineaments density
Airborne magnetic	Units and structural faults that control mineralization frequently have magnetic signatures	Positive magnetic signatures	Airborne magnetic data	(4) TG anomalies
Airborne radiometric	K mobility may be an indicator of fluid remobilization and deposition	K-rich units	Airborne radiometric data	(5) eTh/K map (6) Anomalous K map

Juma District Prospectivity Map

The Juma District prospectivity model delimits regions with the potential to host magmatic–hydrothermal gold and comprises an area of 18,000 km^2 (Figure 7). The six evidential layers were integrated using the fuzzy Gamma operator (set at $\gamma = 0.8$). The prospectivity scores vary from 0 to 0.84, in which the colors range from green to red for the medium to high prospectivity areas (0.39–0.84). The higher values correspond to the most favorable areas to host unknown deposits, as highlighted by warm colors (orange or red). The regions corresponding to lower to medium prospectivity scores (0–0.39) were merged

and, as they do not have a prospective expression in our model, we opted to represent them in gray, reducing the search area to 21.7% of the original extension (3906 km^2).

The results highlighted two targets with known gold occurrences: (1) An elongated N–S region in the northern portion of the map where the cluster of occurrences includes the Guida prospect, and the Chuim granite intrusion outcrops in the south of this area. This prospective zone has a characteristic radiometric signature, marked by a high K. Part of this zone has exploratory geochemistry data coverage, which makes it interesting for follow-up studies. For this reason, we delimited a window, adjacent to the Guida prospect, defined as the Guida Target for assessing the new prospectivity model; (2) an elongated NE–SW zone (~70 km extension) in the southeastern map, spatially related to the major shear zone that cuts the Juma District. Some gold occurrences are aligned with this trend, which extends beyond the study area.

Three target regions without known gold occurrences showed spatial continuity in the highest prospectivity scores. They are located in the westernmost, southeastern, and central Juma District, configuring elongated zones in the NE–SW, E–W, and N–S directions, respectively.

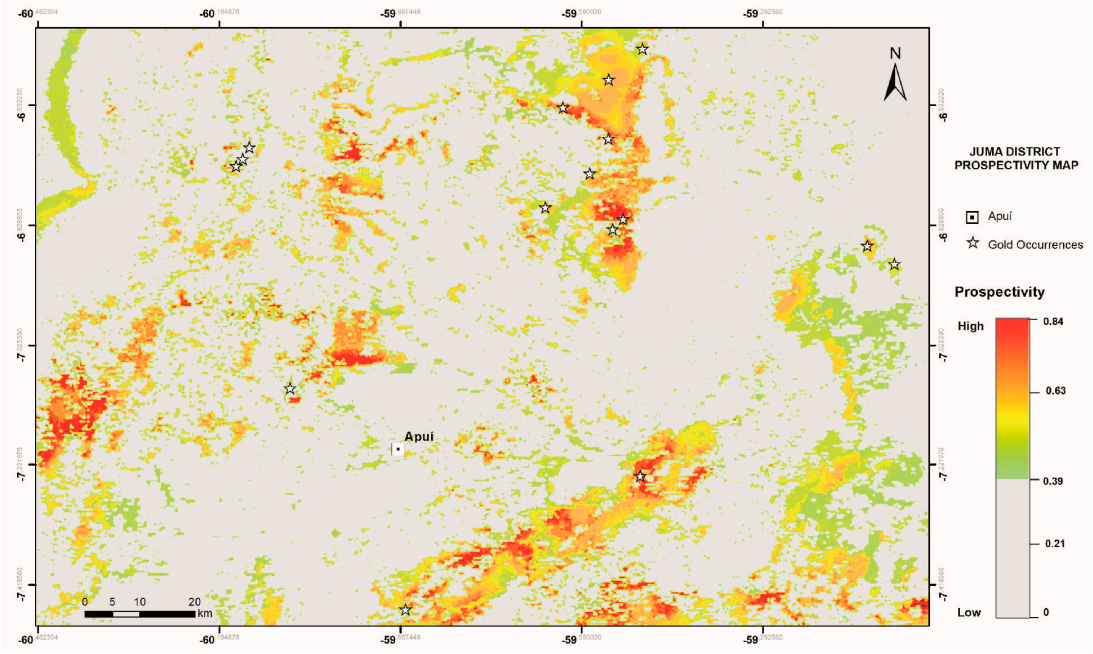


Figure 7. Juma District mineral prospectivity map and known gold occurrences. Regions with similar potential to host magmatic–hydrothermal gold are delimited by the prospectivity scores (0–0.84). The higher values correspond to the most favorable areas (warm colors). The areas corresponding to medium-lower prospectivity scores (0–0.39) are gray.

4.2. Guida Target Gold System and Spatial Proxies

In the Guida Target, the gold is hosted in volcanic and volcano-sedimentary rocks, which are strongly affected by hydrothermalism. The area is adjacent, approximately 5 km, to the Guida and Platô prospects (BBX Minerals), which intersected substantial gold grades in the drill cores, and the Chuim granite outcrops in the southeastern area. In our prospective approach, we consider that the Guida mineralization type could be associated with Paleoproterozoic porphyry–epithermal systems. The Guida Target geometry was defined in this study by considering the targeting results in the Juma District and the coverage of the exploratory geochemistry surveys. The gold system was translated into three system components: source, fluid pathways, and deposition.

To map the source of the gold, we used the basins with heavy mineral concentrate gold anomalies and the lithological units weighted by the potential to host gold. Paleoproterozoic igneous and volcano-sedimentary units related to the Guida mineralization received higher weights. Considering fluid remobilization and hydrothermal alteration as crucial factors for gold deposition in magmatic–hydrothermal systems, the mineralometric data obtained from heavy mineral concentrates were used to identify possible anomalous values of minerals from a hydrothermal origin. Epidote and florencite were strongly correlated with gold occurrences in the Guida Target and their anomalous concentrations in hydrological basins are considered to be spatial proxies. The layers were integrated by the fuzzy OR operator. We also opted to use the highest values in Ce stream sediment analyses as a result of its association with gold occurrences, which is possibly related to the presence of this element in the florencite structure. The positive Ce anomalies were integrated with the anomalous florencite and epidote basins using the fuzzy AND operator. To map fluid migration and depositional processes, we considered that structural weaknesses may act as pathways for hydrothermal fluids. On this scale, local controls, such as minor faults and fractures, were considered for modifying the permeability of the host rocks. We applied the kernel density algorithm to generate two evidential maps for minor and major structures, in which the denser regions are considered the most prospective. These layers were integrated using the fuzzy OR operator. The F factor and Th/K maps also delimited regions with possible hydrothermal remobilization through the K mobility, and their layers were integrated using the fuzzy AND operator. In this scenario, the K enrichment is a key exploratory guide since the strong radiometric responses are spatially related to high hydrothermalized domains. Magnetic units, obtained from the TG, were also considered proxies since both faults and igneous units tend to have magnetic responses. The theoretical fundamentals, spatial proxies, primary data, and evidential maps are characterized by different exploratory criteria in Table 3.

Table 3. Key characteristics describing the theoretical fundamentals, spatial proxies, primary data, and evidential maps in different exploratory criteria for the Guida Target.

Exploratory Criteria	Fundamentals	Spatial Proxy	Primary Data	Evidential Maps
Geological	Paleoproterozoic magmatic systems could be a favorable environment for gold, usually with associated hydrothermal alteration	Host rocks; alteration zones	Juma District geological map; geochronologic data; known gold occurrences	(1) Lithological units weighted by the prospective potential to host gold
Structural	Mineralization is frequently structurally controlled by lineaments, faults, fractures, and contact zones	Proximity to structures	Airborne magnetic data; Juma District geological map	(2) Major lineaments density **OR** Minor lineaments density
Airborne magnetic	Igneous intrusions and structures that control the mineralization usually have magnetic responses	Magnetic signatures	Airborne magnetic data	(3) TG positive anomalies
Airborne radiometric	Potassium mobility may be an indicator of fluid remobilization and ore deposition	K-rich units	Airborne radiometric data survey	(4) F factor map **AND** eTh/K map
Geochemistry	Gold host units are usually enriched with hydrothermal alteration minerals such as epidote and florencite	Proximity to basins with highest values for gold, florencite, and epidote; Ce positive anomalies in stream sediments	Heavy minerals concentrate and stream sediment surveys	(5) Anomalous florencite **OR** epidote basins **AND** Ce highest values basin (6) Basins with the highest values for gold (heavy mineral concentrates)

Guida Target Prospectivity Map

The Guida Target prospectivity map for magmatic–hydrothermal gold was developed on a 1:100,000 scale by integrating six evidential maps using the fuzzy Gamma operator (set at $\gamma = 0.7$). The mineral prospectivity map for the Guida Target (Figure 8) delimits regions with the potential to host magmatic–hydrothermal gold with similar characteristics to porphyry–epithermal systems. The prospectivity scores vary from 0 to 0.85, in which the maximum values correspond to the higher prospectivity, highlighted by warm colors (orange or red). The colors range from green to red in the medium to high prospectivity areas. The areas with low to medium scores (0–0.37) were merged and are represented in gray. The initial search area of 921 km^2 was reduced to 303 km^2 (33% of the original), i.e., only the medium–high favorability classes (3,4,5), which are considered in this study as a priority for follow-up.

The results showed two zones with the highest favorability to host gold: a NE–SW elongated zone in the center of the map, with a 19 km extension, and the southeastern portion of the area containing the Chuim granite. Except for the southwestern portion of the map, where the prospectivity is considered low, the medium to high prospectivity areas are well distributed in the Guida Target, aligned in a NE–SW direction. Some of them have a spatial association with known deposits, such as the Pepita and Tiririca prospects in the southeastern Guida Target.

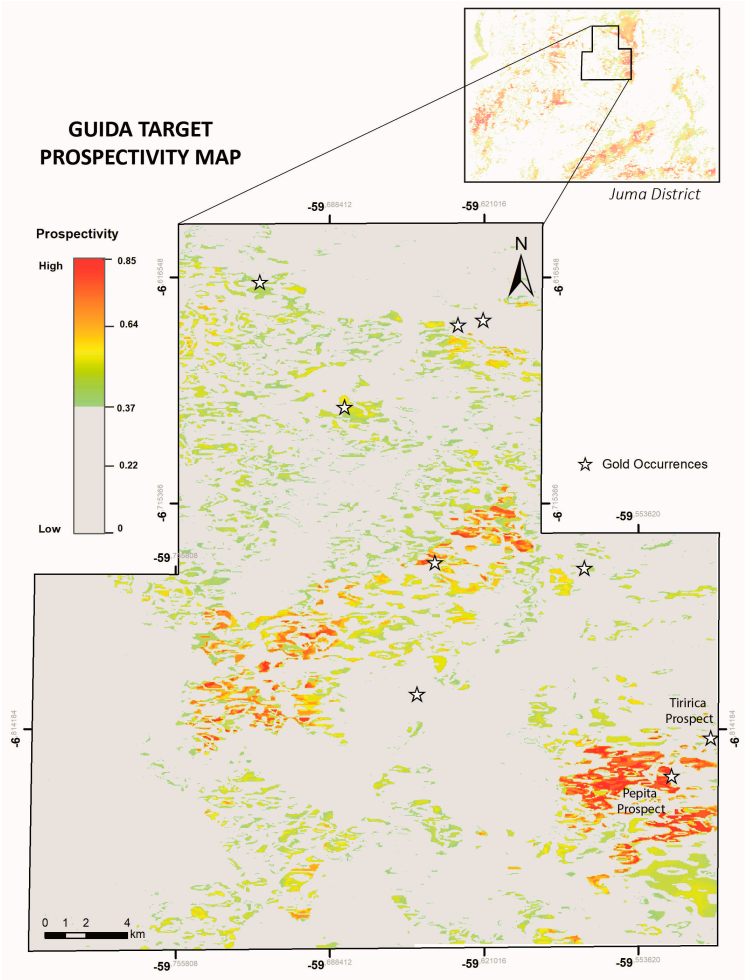


Figure 8. Guida Target mineral prospectivity map and known gold occurrences. Regions with similar potential to host magmatic–hydrothermal gold are delimited by the prospectivity scores (0–0.85). The higher values correspond to the most favorable areas (warm colors). The areas corresponding to medium and low prospectivity scores (0–0.37) are shown in gray.

4.3. Validation of Prospectivity Models

Locations of known mineral deposits of the type sought can be used as an empirical test to evaluate the results of prospectivity modeling and to obtain measures of success [70–72]. It is important to evaluate the prospectivity maps based on how well each map predicts the known gold prospects prior to conducting follow-up work. To evaluate the efficiency of the prospectivity models, we considered the location of 16 primary gold occurrences in the Juma District.

In this research, the efficiency was measured by comparing the number of gold occurrences within each prospectivity class, defined according to the fuzzy scores, to the total area (Figure 9). The prospectivity classes ranged from 1 to 5, where 1 was assigned to the lowest prospectivity regions and 5 to the highest prospectivity areas. The percentage of the cumulative area juxtaposed with the percentage of cumulative gold deposits allowed us to validate the prospectivity models. The plots for the prospectivity models of the Juma District and Guida Target show that, for the Juma District, 71% of the occurrences are mapped in 21.7% of this total area, corresponding to the medium–high prospectivity classes (3–5). For the Guida Target, 56% of the occurrences were mapped in 33% of the Juma District area considering nine gold occurrences. In both cases, a significant reduction in the search area was established by the MPMs.

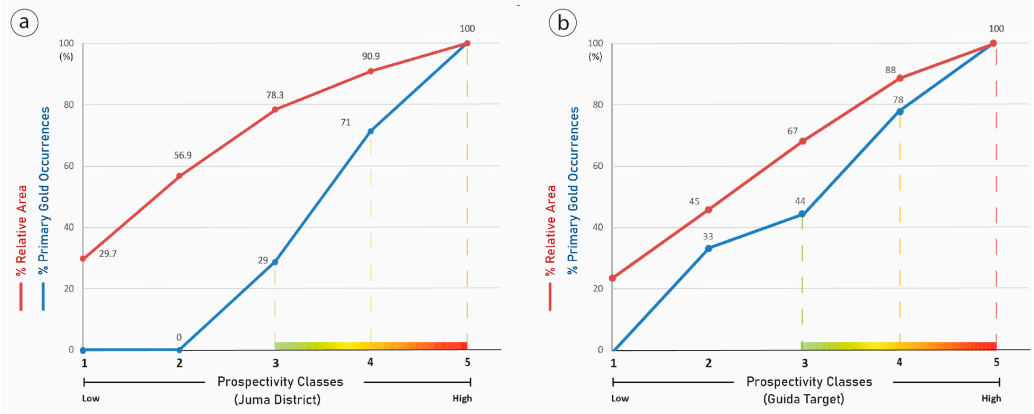


Figure 9. Relative area and gold occurrence percentages plots for the Juma District and Guida Target. The cumulative percentage of primary gold occurrences (blue line) and the cumulative area (red line) for each prospectivity class (1–5); (**a**) Validation for the Juma District prospectivity map; (**b**) Validation for the Guida Target prospectivity map.

4.4. MVI Models

We initially created a regional magnetization model, which covered approximately 97,000 km^2 area, extending beyond the Juma District limits, to facilitate visualizing the continuity of the structures and anomalies. The 1350 m × 1350 m × 700 m cell sizes allowed for the magnetic sources for a 20 km estimated depth to be identified. For the Juma District, a higher resolution magnetization vector inversion was performed with 750 m × 750 m × 350 m cells, aiming to better characterize the targets. The inversions were carried out using grids of the TMI reduced from IGRF, sensitive to both the magnetization and susceptibility of different rocks. The magnetization vector indicates the magnetization degree of a material in response to an applied magnetic field. The dataset was inverted to produce 3D susceptibility models using the Geosoft VOXI Earth Modeling system. The data were inverted subject to a relative error of 2.171 nT (5% of data range). The total field had an approximate intensity of 24,683 nT and an estimated magnetic inclination and declination of −2.66° and −16.51°, respectively. The models were created using unconstrained inversion. The regional MVI inversion was an important technique for investigating the spatial association between the magnetic responses and geologic structures for the Apuí region in 3D. Figure 10 shows the regional model, including the Juma District area, highlighting some of the most significant isosurfaces (surfaces with the same magnetic susceptibility) for gold

exploration. The results showed that the targets delimited by the MPMs frequently have magnetic expressions in the subsurface. High magnetic amplitudes and deep magnetic anomaly sources characterize the main magnetic domain associated with the gold targets in depth. This domain is correlated with the isosurfaces highlighted in Figure 10, with a cutoff of the 3D magnetic susceptibility model showing values greater than 0.001 SI. Geologically, these regions correspond to the Garimpo Eldorado do Juma cluster of occurrences (Juma prospects), the Orosirian Chuim and Arraia granite intrusions (including the Guida prospect), and the NE–SW regional shear zone, which hosts structurally controlled gold deposits. It is also possible to observe the magnetic bodies at shallow depths (<1000 m), some of which were interpreted to be dikes. These magnetic domains traverse the Juma District and have the potential to host gold occurrences in regional and local prospection studies. The magnetic characterization of the NE–SW regional shear revealed that this structure dips toward the northwest at a high angle. This zone has significant volume at depth expanding to the southeast of the Juma District.

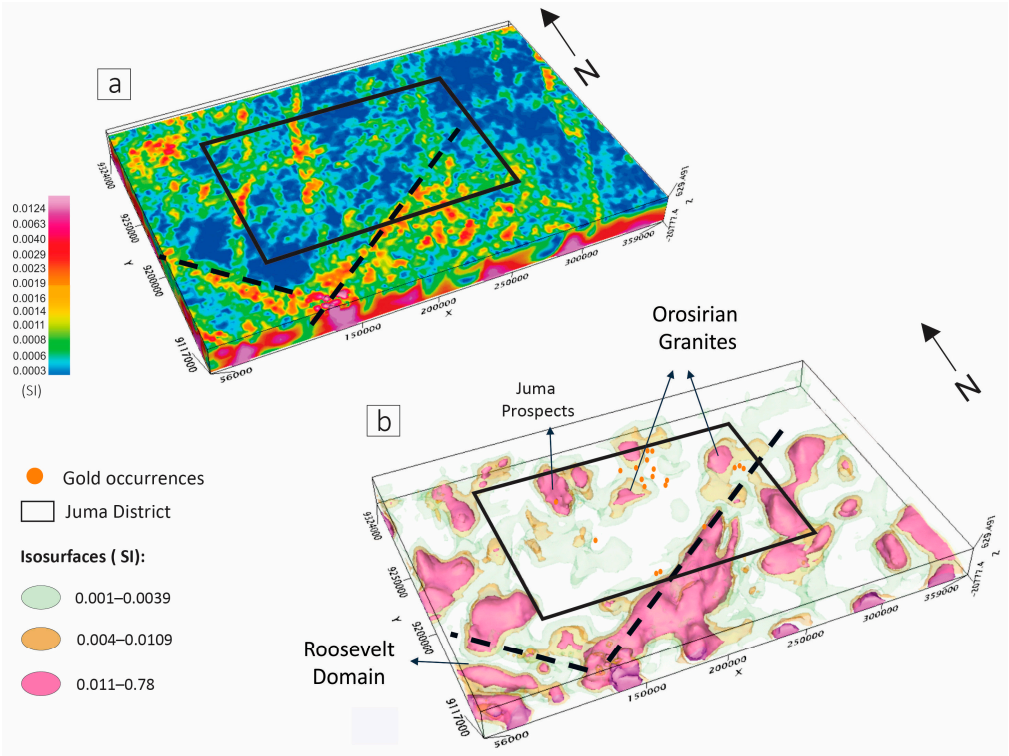


Figure 10. The regional MVI models show: (**a**) the continuity of the magnetic susceptibility in 3D beyond the Juma District limits; (**b**) the most relevant regional isosurfaces and the gold occurrences.

The Juma District MVI model (Figure 11) provided prospective insights on a larger scale for the geophysical–geological interpretation of the main targets. The model highlighted structures and units that could be associated with mineralization at depth. A high-intensity magnetic domain intercepts the surface where the mineralization of the Eldorado do Juma occurs, indicating that the anomalies have deep sources and the gold has a possible geological connection with a deep origin. In this domain, the magnetic susceptibility values are greater than 0.0015 SI. For the Guida prospect, the interpretation was supported by drill cores.

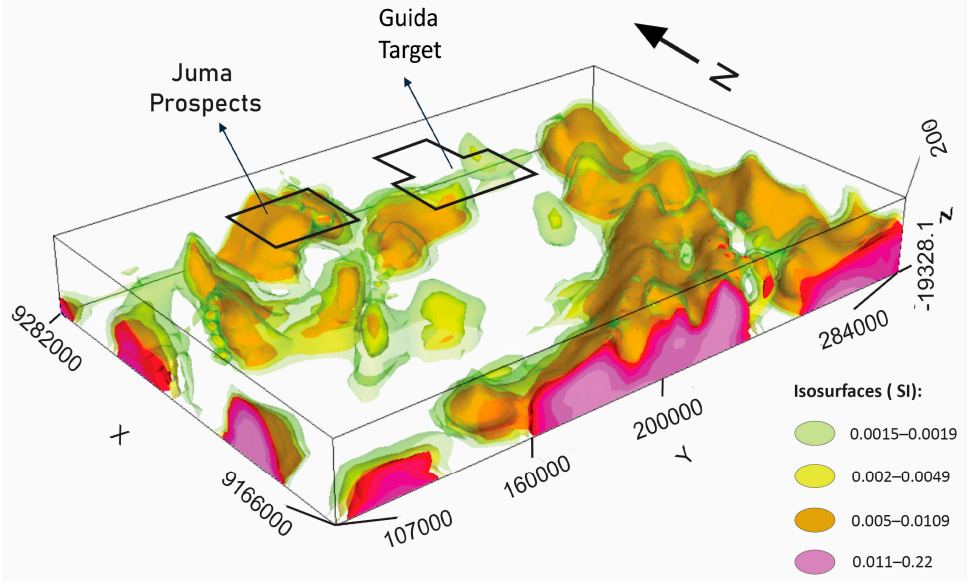


Figure 11. Juma District MVI model with the location of the Guida Target and the Juma prospects areas at a depth of 20 km.

5. Discussion

The evolution of a mineral system can extend over hundreds of millions to billions of years [50]. For mapping the footprints of the mineral system, we considered two different types of gold occurrences in the Juma District and at least three mineralized events, ranging from the Orosirian to Mesoproterozoic, related to magmatic–hydrothermal systems. Although the preservation of porphyry–epithermal mineralization is rare in Proterozoic terrains, several authors have proposed potential for this type of mineralization in the Amazon Craton over the last decades and cases have been described (e.g., [19,73–75]).

For the Juma District, five main targets were defined, three without known gold occurrences. We recommend field investigations in these areas for future exploratory programs. The MVI model highlighted the main magnetic geometries that could be associated with gold mineralization, thus enhancing the regional interpretation of the targets. The NE–SW target in the southeastern portion of the area was characterized by a high-intensity deep magnetic domain that dips toward the northwest at a high angle. This domain extends at depth to the southeast of the Juma District and continues beyond the study area's limits to the south. Because the structures usually control the location and the size of gold deposits, structure-proximal deposits tend to be larger [76]. We considered this domain to be highly promising for regional and local gold prospection since the magnetic responses indicate large structures at depth. However, as a result of the irregular geometry of these anomalies, interpretations without a geological constraint are limited and often qualitative. We suggest constrained inversions for future exploratory studies.

For the Guida Target, the prospectivity map highlighted a NE–SW elongated target, approximately 19 km long, defined as potential for new discoveries. There is one known occurrence in its northeastern portion, but no record of gold deposits in the southwestern portion. Florencite is the most abundant accessory mineral in the regional context and high percentages are frequent in basins with larger amounts of gold, suggesting a metallogenetic association between these minerals. In this study, we defined Florencite and Ce as proxies for hydrothermal alterations associated with gold deposits in the Guida Target region.

Correlation of Results with Known Geology

This topic presents an integrated geological and geophysical interpretation of the results. The joint analysis of six drill holes with MVI data inversion allowed for the definition of guides for future campaigns in the Guida prospect region. The JED–01, JED–02, and JED–03 drill holes intercepted the volcaniclastic breccias, sandstones, tuffs, and

basalts from the Camaiú and Pedro Sara Formations. These rocks are affected by pervasive hydrothermal alteration, mainly sericitization, chloritization, argilitization and carbonation. Intensely oxidized zones are described. The BBX Minerals [77] reported 42.0 g/t Au in the JED–01 hole (Platô prospect) obtained from a 55.25 m composite, reinforcing the gold potential of the Beneficent Group.

The JEDs 04–06 exhibited pervasive hydrothermal alteration features, mainly chloritization, epidotization, and carbonation. The JED–04 and JED–06 predominantly consist of volcano-sedimentary rocks that are intensely altered (Figure 12a) with a cover of saprolitic rocks approximately 50 m thick. Hydrothermal breccias with open cavities and filled with quartz veins (Figure 12b) were present in all drill cores, predominantly close to the granite intrusion. The JED–06 intercepted an apophysis of the Chuim granite at 297 m (Figure 12c). The JED–05 intercepted the Chuim granite, partially altered by sericite, epidote, biotite, and hematite (Figure 12d), after 50 m of saprolitic cover. BBX Minerals reported an average of 3.70 g/t Au in the bottom of hole JED–04 (13.66 m interval), obtained by fire assay analyses [77]. Average values of 37.4 g/t Au were obtained from the bottom 49.44 m (250.00–299.44 m) of hole JED–06 from 12 composite samples of approximately 4 m in length [77]. Two highly significant results of 4.0 m @ 107.11 g/t from 258 m and 4.2 m @ 37.37 g/t from 277.8 m were obtained. Gold is likely to be distributed relatively throughout the lower portion of JED–06.



Figure 12. (**a**) Intensely altered metagrawacke (Abacaxis Fm.) exhibiting quartz veinlets concordant and discordant with foliation in JED–04 at 71 m. (**b**) Breccia with drusiform quartz and open cavities, in JED–04 at 75.5 m. (**c**) Sharp contacts between granite apophysis and the volcano-sedimentary basement, in JED–06 at 297.5 m. (**d**) Chuim granite partially altered by sericite, epidote, biotite, and hematite, in JED–05 at 70.8 m.

All gold intervals had features indicative of a low-sulfidation magmatic–epithermal origin. Breccias and quartz veins with microcrystalline, drusiform, and lattice-bladed textures affect some of the mineralized intervals. It is possible that in a regional context, these occurrences could be related to distal porphyry-epithermal systems; however, detailed metallogenetic studies are required. Using the integrated analyses of several MVI slices combined with the geologic interpretation, we delimited a magnetic surface, defined as the possible contact between the granite intrusion and the volcano-sedimentary sequences. On the basis of the geophysical and geological model, we considered this contact zone to be favorable to the occurrence of new deposits. Figure 13 shows this geometry, represented by the green isosurface, at a magnetic susceptibility of 0.002 SI (see also Video S1, Supplementary Materials). This surface has compatible magnetic susceptibility values with the average for igneous units, related to the mineralization, as granites (0.0025 SI) [78]. We also considered that the hydrothermal breccias and quartz veins occur preferentially close to the contact with the porphyritic Chuim granite based on the drill core logging results.

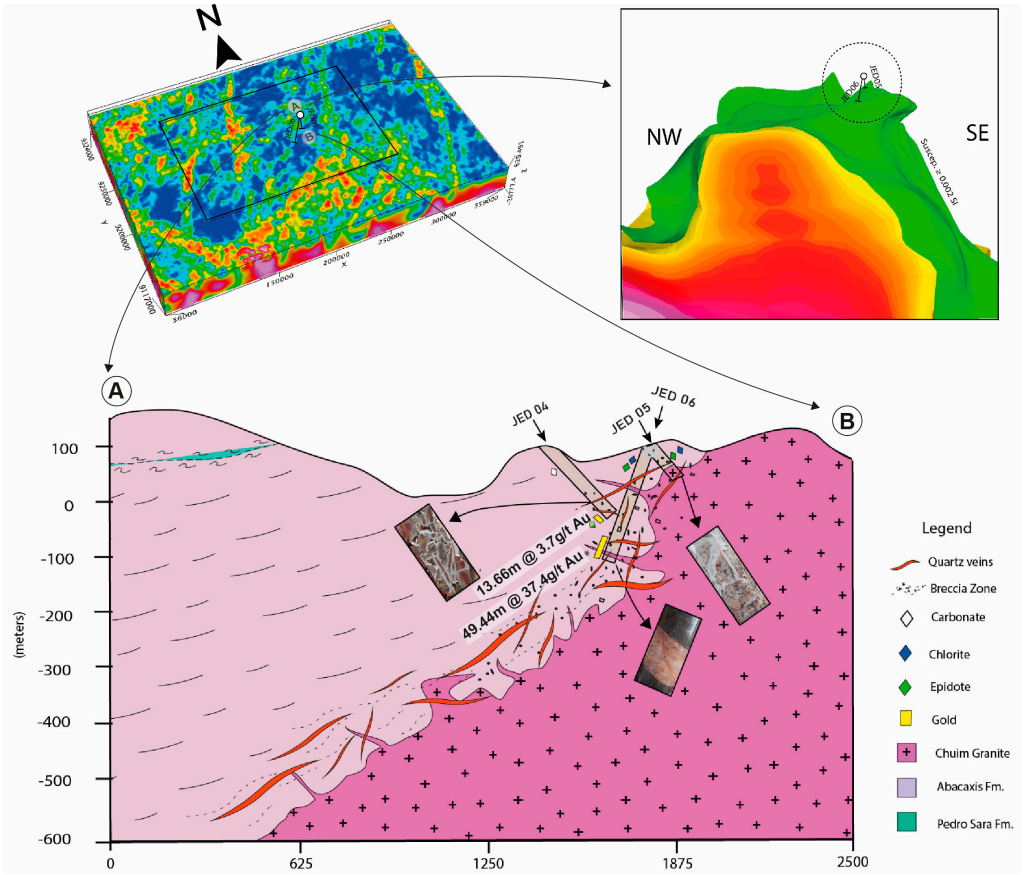


Figure 13. (**A**) Integrated analysis of drill cores (JED–04, JED–05, and JED–06) and the geophysical model for the Guida prospect. (**B**) The isosurface delimited by a 0.002 SI susceptibility was interpreted as the possible contact zone between the Chuim Granite and the volcano-sedimentary sequence. Photographs illustrate intervals from drill cores.

6. Conclusions

This case study provides an overview of the geological setting and gold system for the Apuí region, the Southwestern Amazon Craton, revealing strategies for exploration in regions with intensely weathered cover. A multi-source investigation, using 2D and 3D techniques, resulted in gold prospectivity maps and MVI models for the Juma District and Guida Target. The use of fuzzy logic and magnetic data inversion models revealed key geological, geophysical, geochemical, and structural factors for discovering hidden gold deposits despite the deep cover and limited geological knowledge. Considering the

footprints of the mineral system for a magmatic–hydrothermal exploration model, we defined strategic targets in 2D that were further detailed in 3D. According to the final prospectivity maps, many of the most important known gold deposits were located within areas of high favorability, and other new potential gold targets, without previous gold records, were defined.

This work resulted in the following primary conclusions with respect to gold exploration potential in the Apuí region:

1. The Juma District prospectivity map identified five geologically consistent targets, mostly in NE–SW, E–W, and N–S directions. A significant target, NE–SW aligned, in the southeastern area was characterized in 3D as a magnetic domain that extends to the southeast and dips toward the northwest. We believe that this target should be prioritized for further investigation programs;
2. The Guida Target prospectivity map defined two main targets. The first is in the southeastern area, containing the Chuim granite. The other is a NE–SW elongated zone in the central area in which the continuity for the southwest is considered favorable for gold prospection;
3. Using the integrated analyses of several MVI slices and the geologic interpretation of the drill cores, we characterized a surface, defined as the contact zone, between the granite intrusion and the volcano-sedimentary sequence, which is considered to be favorable to the occurrence of new deposits at depth;
4. In this study, we collected airborne geophysical and exploratory geochemical data that will help to improve the exploration pipeline and future 2D and 3D prospectivity mapping;
5. The amount of gold produced in the Juma District and the results presented in this work point to an unexplored potential for economic magmatic–hydrothermal gold deposits in the Apuí region;
6. This study presents new approaches for mineral exploration in undercover terrains and can be used as an exploration guide for similar deposits in a regional context.

Supplementary Materials: The following supporting information can be downloaded at: https://www.mdpi.com/article/10.3390/min13010078/s1. Table S1: Geochronological data for the Southern Amazon Craton; Table S2: Statistical summary of some elements considered relevant for Au deposits; Video S1: MVI model for the Guida prospect.

Author Contributions: Conceptualization of the research project (master thesis, UnB), L.C.Q. and A.M.S.; Geochemistry analysis M.Z.P.; MVI modeling, F.R.F.R.d.O.e.S.; Regional geology, M.A.M.; Writing—Original Draft Preparation, L.C.Q.; Reviewing and Editing, M.Z.P.; Supervision, A.M.S. All authors have read and agreed to the published version of the manuscript.

Funding: This research received no external funding.

Data Availability Statement: The data presented in this study are available in this paper and in the Geological Survey of Brazil repository.

Acknowledgments: The authors would like to thank the Geological Survey of Brazil (GSB/CPRM) for their support, including the study time-off granted to researcher Lila Queiroz. We would also like to thank BBX Minerals for providing the drill cores for analysis and CAPES for the Portal de Períodicos. Lila Queiroz also recognizes the support of Marina N. Ramos, Antonia Railline da C. Silva, Raul E. Meloni, Tomas M. Lisboa, and Matheus S. Simões for technical discussions and contributions. Adalene M. Silva would like to thank CNPq for the research productivity grant (Process 311565/2018-2).

Conflicts of Interest: The authors declare no conflict of interest.

References

1. Wyborn, L.A.I.; Heinrich, C.A.; Jaques, A.L. Australian Proterozoic Mineral Systems: Essential Ingredients and Mappable Criteria. In Proceedings of the Australasian Institute of Mining and Metallurgy Publication Series, Darwin, Australia, 5–9 August 1994; Volume 94, pp. 109–115.
2. Hronsky, J.M.A.; Groves, D.I. Science of targeting: Definition, strategies, targeting and performance measurement. *Aust. J. Earth Sci.* **2008**, *55*, 3–12. [CrossRef]
3. McCuaig, T.C.; Hronsky, J.M.A. The mineral system concept: The key to exploration targeting. *Soc. Econ. Geol. Special Pub.* **2014**, *18*, 153–176. [CrossRef]
4. Carranza, E.J.M. Natural Resources Research publications on geochemical anomaly and mineral potential mapping, and introduction to the special issue of papers in these fields. *Nat. Resour. Res.* **2017**, *26*, 379–410. [CrossRef]
5. Kreuzer, O.P.; Yousefi, M.; Nykänen, V. Introduction to the special issue on spatial modelling and analysis of ore-forming processes in mineral exploration targeting. *Ore Geol. Rev.* **2020**, *119*, 103391. [CrossRef]
6. Shirazy, A.; Ziaii, M.; Hezarkhani, A.; Timkin, T. Geostatistical and Remote Sensing Studies to Identify High Metallogenic Potential Regions in the Kivi Area of Iran. *Minerals* **2020**, *10*, 869. [CrossRef]
7. Yousefi, M.; Carranza, E.J.M.; Kreuzer, O.P.; Nykänen, V.; Hronsky, J.M.A.; Mihalasky, M.J. Data analysis methods for prospectivity modelling as applied to mineral exploration targeting: State-of-the-art and outlook. *J. Geochem. Explor.* **2021**, *229*, 106839. [CrossRef]
8. González-Álvarez, I.; Goncalves, M.A.; Carranza, E.J.M. Challenges for Mineral Exploration in the 21st Century: Targeting Mineral Deposits Under Cover. *Ore Geol. Rev.* **2020**, *126*, 103785. [CrossRef]
9. Joly, A.; Porwal, A.; McCuiag, T.C. Exploration targeting for orogenic gold deposits in the Granites- Tanami Orogen: Mineral system analysis, targeting model and prospectivity analysis. *Ore Geol. Rev.* **2012**, *48*, 349–383. [CrossRef]
10. Bonham-Carter, G.F. Geographic information systems for geoscientists—Modeling with GIS. *Comput. Methods Geosci.* **1994**, *13*, 398.
11. Porwal, A.; Das, R.D.; Chaudhary, B.; Gonzalez-Alvarez, I.; Kreuzer, O. Fuzzy inference systems for prospectivity modeling of mineral systems and a case-study for prospectivity mapping of surficial Uranium in Yeelirrie Area, Western Australia. *Ore Geol. Rev.* **2015**, *71*, 839–852. [CrossRef]
12. Assumpção, M.; Bianchi, M.; Julia, J.; Dias, F.L.; França, G.S.; Nascimento, R.; Drouet, S.; Pavão, C.G.; Albuquerque, D.F.; Lopes, A.E.V. Crustal thickness map of Brazil: Data compilation and main features. *J. South Am. Earth Sci.* **2013**, *43*, 74–85. [CrossRef]
13. Costa, J.W.C.; Costa, J.W.C.; Fuck, R.A. The structure of the Amazonian craton: Available geophysical evidence. *J. South Am. Earth Sci.* **2016**, *70*, 162–173. [CrossRef]
14. Albuquerque, D.F.; Sand, G.; Paes, L.; Bianchi, M.; Vieira, L.; Assumpção, M.; Condori, C.; Estrela, M. Crustal structure of the Amazonian Craton and adjacent provinces in Brazil. *J. South Am. Earth Sci.* **2017**, *79*, 431–442. [CrossRef]
15. Lloyd, S.; van der Lee, S.; França, G.S.; Assumpção, M.; Feng, M. Moho map of South America from receiver functions and surface waves. *J. Geophys. Res.* **2010**, *115*, B11315. [CrossRef]
16. Meloni, R.E.; Simões, M.S.; Benevides, P.R.R. Granitos de idade orosiriana no limite entre as províncias Tapajós-Parima e Rondônia-Juruena, região de Apuí-AM. In Proceedings of the 49° Congresso Brasileiro de Geologia, Rio de Janeiro, Brazil, 20–24 August 2018; Sociedade Brasileira de Geologia: São Paulo, Brazil, 2018.
17. Simões, M.S.; Meloni, R.E.; Santos, J.O.S. Stratigraphy, depositional environments and zircon U-Pb (LA-ICP-MS) ages of the Statherian volcano-sedimentary Beneficente Group: Implications for tectonics and gold mineralization in SW of the Amazon Craton. *Precambrian Res.* **2020**, *345*, 0301–9268. [CrossRef]
18. Meloni, R.E.; Simões, M.S.; Oliveira, A.C.S. Áreas de relevante interesse mineral (ARIM): Evolução crustal e metalogenia do sudeste do Amazonas: Distrito aurífero Juma, estado do Amazonas. In *Informe de Recursos Minerais—Série Províncias Minerais do Brasil*; Meloni, R.E., Simões, M.S., Oliveira, A.C.S., Eds.; CPRM—Serviço Geológico do Brasil: Manaus, Brazil, 2021; Volume 34, p. 315.
19. Moura, M.A.; Botelho, N.F.; Olivo, G.R.; Kyser, T.K. Granite-related Paleoproterozoic, Serrinha gold deposit, Southern Amazonia, Brazil: Hydrothermal alteration, fluid inclusion and stable isotope constraints on genesis and evolution. *Econ. Geo.* **2006**, *101*, 585–605. [CrossRef]
20. Juliani, C.; Vasquez, M.L.; Klein, E.L.; Villas, R.N.N.; Echeverri-Misas, C.M.; Santiago, E.S.B.; Monteiro, L.V.S.; Carneiro, C.C.; Fernandes, C.M.D.; Usero, G. Metalogenia da Província Tapajós. In *Metalogênese das Províncias Tectônicas Brasileiras*; Silva, M.G., Neto, M.G.R., Jost, H., Kuyumajian, R.M., Eds.; CPRM—Serviço Geológico do Brasil: Belo Horizonte, Brazil, 2014; Volume 1, pp. 229–268.
21. Juliani, C.; de Assis, R.R.; Monteiro, L.V.S.; Fernandes, C.M.D.; da Silva Martins, J.E.Z.; Ricardo Costa e Costa, J. Gold in Paleoproterozoic (2.1 to 1.77 Ga) Continental Magmatic Arcs at the Tapajós and Juruena Mineral Provinces (Amazonian Craton, Brazil): A New Frontier for the Exploration of Epithermal–Porphyry and Related Deposits. *Minerals* **2021**, *11*, 714. [CrossRef]
22. Almeida, F.F.M.; Hasui, Y. O embasamento da Plataforma Sul Americana. In *O Pré-Cambriano do Brasil*, 1st ed.; Blucher: São Paulo, Brazil, 1984; p. 378.
23. Almeida, F.F.M. Tectonic Map of South America, 1:5,000,000. In *Explanatory Note*; Almeida, F.F.M., Ed.; DNPM/CGMW/UNESCO: Brasília, Brasil, 1978; p. 23.

24. Almeida, F.F.M.; Brito Neves, B.B.; Carneiro, C.D.R. The origin and evolution of the South American Platform. *Earth Sci. Rev.* **2000**, *50*, 77–111. [CrossRef]
25. Tassinari, C.C.G.; Macambira, M.J.B. A evolução tectônica do Craton Amazônico. In *Geologia do Continente Sul Americano: Evolução da Obra de Fernando Flávio Marques Almeida*; Neto, V.M., Bartorelli, A., Carneiro, C.D.R., Neves, B.B.B., Eds.; BECA: São Paulo, Brazil, 2004; pp. 471–486.
26. Cordani, U.G.; Teixeira, W. Proterozoic accretionary belt in the Amazonian Craton. *Geol. Soc. Am. Mem.* **2007**, *200*, 297–320.
27. Scandolara, J.E.; Correa, R.T.; Fuck, R.A.; Souza, V.S.; Rodrigues, J.B.; Ribeiro, P.S.E.; Frasca, A.A.S.; Saboia, A.M.; Lacerda Filho, J.V. Paleo-Mesoproterozoic arc-accretion along the southwestern margin of the Amazonian craton: The Juruena accretionary orogen and possible implications for Columbia supercontinent. *J. S. Am. Earth Sci.* **2017**, *73*, 223–247. [CrossRef]
28. Tassinari, C.C.G.; Macambira, M.J.B. Geochronological Provinces of the Amazonian Craton. *Episodes* **1999**, *22*, 174–182. [CrossRef] [PubMed]
29. Santos, J.O.S.; Hartman, L.A.; Gaudette, H.E.; Groves, D.I.; McNaughton, N.; Fletcher, I.R. A new understanding of the provinces of the Amazon craton based on integration of field mapping and U-Pb and Sm-Nd geochronology. *Gondwan Res.* **2000**, *3*, 453–488. [CrossRef]
30. Bonvalot, S.; Balmino, G.; Briais, A.; Huhn, M.; Peyrefitte, A.; Vales, N.; Biancale, R.; Gabalda, G.; Moreaux, G.; Reinquin, F.; et al. World Gravity Map Scale 1:50,000,000. In *World Gravity Map Explanatory Note*, 1st ed.; CGMW—(Commission for the Geological Map of the World), Ed.; BGI; CNES; IRD: Paris, France, 2012.
31. Santos, J.O.S.; Rizzotto, G.J.; Potter, P.E.; McNaughton, N.J.; Matos, R.S.; Hartmann, L.A.; Chemale, F., Jr.; Quadros, M.E.S. Age and autochthonous evolution of the Sunsás Orogen in West Amazon Craton based on mapping and U-Pb geochronology. *Precambr. Res.* **2008**, *165*, 120–152. [CrossRef]
32. Lacerda Filho, J.V.; Souza, J.O.; Oliveira, C.C.; Ribeiro, P.S.E.; Boas, P.F.V.; Albuquerque, M.C.; Frasca, A.A.S.; Borges, F.R.; Moreton, L.C.; Martins, E.G.; et al. Geologia e Evolução Tectônica da Região Norte do Mato Grosso (Projeto Promin-Alta Floresta). In Proceedings of the Simpósio de Geologia da Amazônia, Belém, Brazil, 4–9 November 2001; Sociedade Brasileira de Geologia: Belém, Brazil, 2001.
33. Souza, J.P.; Frasca, A.A.S.; Oliveira, C.C. Geologia e Recursos Minerais da Província Mineral de Alta Floresta. Relatório Integrado. In *Programa Levantamentos Geológicos Básicos do Brasil (Projeto Província Mineral de Alta Floresta)*; CPRM-Serviço Geológico do Brasil: Goiânia, Brazil, 2005; Volume 1, p. 159.
34. Simões, M.S.; Meloni, R.E.; Benevides Filho, P.R.R.; Lisboa, T.M.; Silva, A.R.C. A sucessão vulcanossedimentar dos grupos Colíder e Beneficente no sudeste do Amazonas: Estilos eruptivos, tipos composicionais e ambientes de sedimentação. *Contrib. À Geol. Da Amaz.* **2017**, *10*, 263–272.
35. Bizinella, G.A.; Santiago, A.F.; Melo, A.F.F.; Santos, A.; Borges, F.R.; Godoy, H.K.; Yamaguti, H.S.; Oliveira, J.R.; Carmona, J.R.M.; D'Antona, R.J.G.; et al. *Projeto Tapajós—Sucunduri, Relatório Inédito*; Ministério das Minas e Energia, Convênio DNPM/CPRM: Brasília, Brazil, 1980.
36. Oliveira, A.C.S.; Almeida, M.E. Faixa deformacional Roosevelt-Guariba: Evento tectono termal calimiano intracratônico no sudeste do Amazonas, porção sudoeste do Cráton Amazonas. In Proceedings of the XVII Simpósio Nacional de Estudos Tectônicos, Bento Gonçalves, Brazil, 26–29 June 2019.
37. Betiollo, L.M.; Reis, N.J.; Almeida, M.E.; Bahia, R.B.C.; Splendor, F.; Costa, U.A.P.; Luzardo, R. Magmatismo Máfico Calimiano (Sill Mata-Matá), rio Aripuanã, Amazonas—Implicações Geológicas. In Proceedings of the XI Simpósio de Geologia da Amazônia, Manaus, Brazil, 25 September 2009; Sociedade Brasileira de Geologia: Manaus, Brazil, 2009.
38. Meloni, R.E.; Simões, M.S. As mineralizações de ouro do Distrito Aurífero Juma-SE do Amazonas. In Proceedings of the IV Simpósio de Metalogenia, Gramado-RS, Brazil, 10 April 2019.
39. Moura, M.; Botelho, N. Petrologia do magmatismo associado à mineralização do tipo ouro pórfiro da Província Aurífera Juruena–Teles Pires (MT). *Rev. Bras. Geociências* **2002**, *32*, 377–386. [CrossRef]
40. Moura, M.A. O maciço Granítico Matupá e o Depósito de Ouro Serrinha (MT): Petrologia, Alteração Hidrotermal e Metalogenia. Ph.D. Thesis, Universidade de Brasília, Brasília, Brazil, 1998.
41. Castro, A.A. Gênese do Depósito de ouro Tocantinzinho, Província Mineral Tapajós (Pará): Evidências a partir de dados de Geologia, Petrologia e Inclusões Fluidas. Master's Thesis, Instituto de Geociências da Universidade de Brasília, Brasília, Brazil, 2015.
42. Lopes, A.A.C.; Moura, M.A. The Tocantinzinho Paleoproterozoic Porphyry-Style Gold Deposit, Tapajos Mineral Province (Brazil): Geology, Petrology and Fluid Inclusion Evidence for Ore-Forming Processes. *Minerals* **2019**, *9*, 29. [CrossRef]
43. Sillitoe, R.H. Intrusion-related gold deposits. In *Gold Metallogeny and Exploration*; Foster, R.P., Ed.; Blackie: Glasgow, Scotland, 1991; pp. 165–209.
44. Sillitoe, R.H. Gold-rich porphyry copper deposits: Geological model and exploration implications. *Geol. Assoc. Can. Spec. Pap.* **1993**, *40*, 465–478.
45. Sillitoe, R.H. Gold-rich porphyry deposits: Descriptive and genetic models and their role in exploration and discovery. *Rev. Econ. Geol.* **2000**, *13*, 315–345.

46. Sillitoe, R.H. Porphyry copper systems. *Econ. Geol.* **2010**, *105*, 3–41. [CrossRef]
47. Hedenquist, J.W.; Lowenstern, J.B. The role of magmas in the formation of hydrothermal ore deposits. *Nature* **1994**, *370*, 519–527. [CrossRef]
48. Brito, R.S.; Silveira, F.V.; Larizzati, J.H. Metalogenia do Distrito Aurífero do rio Juma—Nova Aripuanã—AM. In *Informe de Recursos Minerais—Série Ouro*; CPRM—Serviço Geológico do Brasil: Brasília, Brazil, 2010; Volume 17, p. 35.
49. Goulart, L.E.A.; Silva, A.R.d.C. Metalogenia das províncias minerais do Brasil: Área Eldorado do Juma, estado do Amazonas. In *Informe de recursos minerais—Série províncias minerais do Brasil*; CPRM—Serviço Geológico do Brasil: Manaus, Brazil, 2021; Volume 10, p. 99.
50. Hagemann, S.G.; Lisitsin, V.; Huston, D.L. Mineral system analysis: Quo Vadis. *Ore Geol. Rev.* **2016**, *76*, 504–522. [CrossRef]
51. Pan, G.; Harris, D.P. *Information Synthesis for Mineral Exploration*, 1st ed.; Oxford University Press: New York, NY, USA, 2000; p. 461.
52. Harris, J.R.; Sanborn-Barrie, M.; Panagapko, D.; Skulski, T.; Parker, J.R. Gold prospectivity maps of the Red Lake greenstone belt: Application of GIS technology. *Can. J. Earth Sci.* **2006**, *43*, 865–893. [CrossRef]
53. Nykänen, V.M. *Spatial data analysis as a tool for mineral prospectivity mapping*, 1st ed.; GTK: Espoo, Finland, 2008; Volume 76, p. 4.
54. Silva, E.C.; Silva, A.M.; Toledo, C.L.B.; Mol, A.G.; Otterman, D.W.; Souza, S.R.C. Mineral Potential Mapping for Orogenic Gold Deposits in the Rio Maria Granite Greenstone Terrane, Southeastern Pará State, Brazil. *Econ. Geol.* **2012**, *107*, 1387–1402. [CrossRef]
55. Uchôa, J.C.F.; Toledo, C.L.B.; Silva, A.M.; Mendonça, A.F.; Hagemann, S.G.; Kreuzer, O.P.; Carmelo, A. Multi-process and multi-scale spatial predictive analysis of an orogenic Archean gold system, Rio das Velhas Greenstone Belt, Brazil. *Ore Geol. Rev.* **2020**, *122*, 103442. [CrossRef]
56. Pitarello, M.Z.; Meloni, R.E.; Simões, M.S. Mapeamento Geoquímico de Sedimento de Corrente no Distrito Juma, Sudeste do Amazonas. In Proceedings of the XVI Simpósio de Geologia da Amazônia, Manaus, Brazil, 11 October 2019; Sociedade Brasileira de Geologia: Manaus, Brazil, 2019.
57. Akima, H. A new method of interpolation and smooth curve fitting based on local procedures: New York, NY, USA. *J. Assoc. Comput. Mach.* **1970**, *7*, 1–14.
58. Smith, W.H.F.; Wessel, P. Gridding with continuous curvature splines in Tension. *Geophysics* **1990**, *55*, 293–305. [CrossRef]
59. Efimov, A.V. Multiplikativnyj pokazatel dlja vydelenija endogennych rud poaerogamma-spektrometriceskim dannym. In *Metody Rudnoj Geofiziki*, 1st ed.; Naucno-proizvodstvennoje Objedinenie Geofizika: Leningrad, Russia, 1978; pp. 59–68.
60. Pires, A.C.B. Identificação geofísica de áreas de alteração hidrotermal, Crixás-Guarinos, Goiás. *Rev. Bras. De Geociências* **1985**, *25*, 61–68. [CrossRef]
61. Carranza, E.J.M. Analysis and mapping of geochemical anomalies using logratio- transformed stream sediment data with censored values. *J. Geochem. Explor.* **2011**, *110*, 167–185. [CrossRef]
62. Carranza, E.J.M. Geochemical anomaly and mineral prospectivity mapping in GIS. In *Handbook of Exploration and Environmental Geochemistry*, 1st ed.; Elsevier: Amsterdam, The Netherlands, 2008; p. 347.
63. Filzmoser, P.; Hron, K.; Reimann, C. Univariate statistical analysis of environmental (compositional) data: Problems and possibilities. *Sci. Total Environ.* **2009**, *407*, 6100–6108. [CrossRef]
64. Grunsky, E.C. The interpretation of geochemical survey data. *Geochem. Explor. Environ. Anal.* **2010**, *10*, 27–74. [CrossRef]
65. Reimann, C.; Filzmoser, P.; Garrett, R.G.; Dutter, R. *Statistical Data Analysis Explained: Applied Environmental Statistics with R*, 1st ed.; John Wiley & Sons: Chichester, UK, 2008; p. 343.
66. Zadeh, L.A. Fuzzy sets. *Inf. Control* **1965**, *8*, 38–353. [CrossRef]
67. Raines, G.L.; Sawatzky, D.L.; Bonham-Carter, G.F. *New Fuzzy Logic Tools in ArcGis*, 10th ed.; ESRI: Redlands, CA, USA, 2010; p. 13.
68. Ellis, R.G.; de Wet, B.; Macleod, I.N. Inversion of magnetic data for remanent and induced sources. In Proceedings of the 22nd Australian Society of Exploration Geophysicists (ASEG), Brisbane, Australia, 10 November 2012.
69. Couto, M.A., Jr.; Aisengart, T.; Barbosa, D.; Ferreira, R.C.R.; Baltazar, O.F.; Marinho, M.S.; Cavalcanti, J.A.D.; Araújo, J.C.S. Magnetization Vector Inversion Application in Quadrilatero Ferrifero Region, MG, Brazil. *SEG Glob. Meet. Abstr.* **2017**, 523–528.
70. Agterberg, F.P.; Bonham-Carter, G.F. Measuring the Performance of Mineral-Potential Maps. *Nat. Resour. Res.* **2005**, *14*, 1–17. [CrossRef]
71. Nykänen, V.; Lahti, I.; Niiranen, T.; Korhonen, T. Receiver operating characteristics (ROC) as validation tool for prospectivity models—A magmatic Ni–Cu case study from the Central Lapland Greenstone Belt, Northern Finland. *Ore Geol. Rev.* **2015**, *71*, 853–860. [CrossRef]
72. Parsa, M.; Maghsoudi, A.; Yousefi, M.; Sadeghi, M. Prospectivity modeling of Porphyry-Cu deposits by identification and integration of efficient mono-elemental geochemical signatures. *J. Afr. Earth Sci.* **2016**, *114*, 228–241. [CrossRef]
73. Coutinho, M.G.d.N.; Robert, F.; dos Santos, R.A. A first approach in understanding the gold mineralization of Tapajós Mineral Province, Amazonian area, Brazil. In Proceedings of the 10th International Gold Symposium; Minérios & Minerales, Rio de Janeiro, Brazil, 29–30 September 1997.
74. Usero, G.; Juliani, C.; Bello, R.D.S.; Echeverri-Misas, C.M.; Tommasini, D.; Monteiro, L.V.S. Estudo das inclusões fluidasmineralização paleoproterozoica de Au–(Cu) do tipo pórfiro do Palito, Província Aurífera do Tapajós (PA). In *Contribuições à Metalogenia do Brasil*; Frantz, J.C., Marques, J.C., Jost, H., Eds.; UFRGS/Instituto de Geociências: Porto Alegre, Brazil, 2011; Volume 1, pp. 111–128.

75. Poggi, L.; Ducart, D.F.; Mesquita, M.J.; Moreira, I.C.; Gomes, M.E.B.; de Souza Filho, C.R. New Insights into the Evolution and Footprints of the Paraíba Au-Cu-Mo Deposit, Alta Floresta Mineral Province (Brazil), through Integration of Spectral and Conventional Methods. *Minerals* **2022**, *12*, 1327. [CrossRef]
76. Groves, D.I.; Santosh, M.; Zhang, L. A scale-integrated exploration model for orogenic gold deposits based on a mineral system approach. *Geosci. Front.* **2000**, *11*, 719–738. [CrossRef]
77. Bbx Minerals. Available online: https://www.bbxminerals.com/pdf/cf6a929e-bc5f-4485-a288-153c66a727b4/Half-Year-Accounts.pdf (accessed on 25 December 2022).
78. Telford, W.M.; Geldart, L.P.; Sheriff, R.E. *Applied Geophysics*, 2nd ed.; Cambridge University Press: Cambridge, UK, 1990; p. 770.

Disclaimer/Publisher's Note: The statements, opinions and data contained in all publications are solely those of the individual author(s) and contributor(s) and not of MDPI and/or the editor(s). MDPI and/or the editor(s) disclaim responsibility for any injury to people or property resulting from any ideas, methods, instructions or products referred to in the content.